photonics

MDPI

Communication

Scaling Law of THz Yield from Two-Color Femtosecond Filament for Fixed Pump Power

Irina A. Nikolaeva [1,2], Daniil E. Shipilo [1,2], Nikolay A. Panov [1,2], Weiwei Liu [3], Andrei B. Savel'ev [1,2] and Olga G. Kosareva [1,2,*]

[1] Faculty of Physics, M. V. Lomonosov Moscow State University, 1/62 Leninskie Gory, 119991 Moscow, Russia
[2] P. N. Lebedev Physical Institute of the Russian Academy of Sciences, 53 Leninskiy Prospect, 119991 Moscow, Russia
[3] Tianjin Key Laboratory of Micro-Scale Optical Information Science and Technology, Institute of Modern Optics, Nankai University, Tianjin 300350, China
* Correspondence: kosareva@physics.msu.ru

Abstract: In 3*D* + time numerical simulations, we study the wavelength scaling law for the energy of terahertz (THz) radiation emitted from a two-color femtosecond filament, which forms during cofocusing into air the fundamental and second harmonics of the laser pulse. In our simulations, the central wavelength of the fundamental harmonic varied from 0.8 to 8 μm and the numerical aperture varied from 0.006 to 0.03. While the harmonics and supercontinuum development are not extreme, so the harmonics spectra are clearly separated, the energy of the generated THz radiation is proportional to the oscillation energy of the electrons, which grows as the squared pump wavelength, and the total number of free electrons in the filament, which decreases quasi-exponentially with the pump wavelength. As a result, the scaling law for the THz energy on the pump wavelength is nonmonotonic with the maximum at 1.6–4 μm depending on the focusing conditions.

Keywords: femtosecond filamentation; terahertz radiation; infrared supercontinuum

Citation: Nikolaeva, I.A.; Shipilo, D.E.; Panov, N.A.; Liu, W.; Savel'ev, A.B.; Kosareva, O.G. Scaling Law of THz Yield from Two-Color Femtosecond Filament for Fixed Pump Power. *Photonics* **2022**, *9*, 974. https://doi.org/10.3390/photonics9120974

Received: 7 November 2022
Accepted: 9 December 2022
Published: 12 December 2022

1. Introduction

Infrared femtosecond pulses are recognized in spectroscopy (both linear [1] and nonlinear [2]), electron acceleration [3], high-order harmonic generation [4,5], atmospheric science [6,7], etc. Two-color (with two carrier frequencies ω_0 and $2\omega_0$ corresponding to wavelengths λ_0 and $\lambda_0/2$) air-based mid-infrared (MIR) plasma THz sources [8] have been shown to be more efficient as compared with the near-infrared ones [9]. The extremely energetic sub-mJ THz pulses emitted from two-color MIR filaments predicted theoretically in [10,11] were experimentally observed recently [12–14]. The THz fields in such pulses are sufficient to study the effects of nonlinear THz photonics [15]. These powerful low-frequency pulses can be applied in THz communications [16] and THz remote sensing of the atmosphere [17].

The ponderomotive potential of a free electron in an electromagnetic wave is proportional to the squared wavelength λ_0^2. Therefore, one can expect that the energy W_{THz} of the THz radiation emitted from the two-color filament is proportional to λ_0^2 as well. This idea was checked experimentally in [8,18]. The measured dependencies of the THz yield on the pump wavelength λ_0, usually referred as THz energy *scaling laws*, increase much faster than the squared wavelength λ_0: the fit of the measured dependencies using the power function $W_{\mathrm{THz}} \propto \lambda_0^{\alpha}$ provides $\alpha = 4.6 \pm 0.5$ [8] and $\alpha = 5.6$–14.3 [18]. The 3*D* + time simulations [18] reproduced these faster than λ_0^2-scaling laws and explained such dependencies by the variation of the relative phase φ between ω_0- and $2\omega_0$-pulses at the output of the frequency-doubling crystal, as well as the dependence of the laser beam size and duration at the output of the optical parametric amplifier on the generated wavelength λ_0.

The λ_0^{α}-trend should not be treated as universal or global since the measured dependencies $W_{\mathrm{THz}}(\lambda_0)$ are nonmonotonic [19] and saturate or even decrease significantly in the long-wavelength region [8,18]. This decrease of the THz yield for a long-wavelength pump was explained by the decrease in the plasma density in [8]. However, in [18], this effect was associated with the variation of the relative phase φ between the harmonics. The measurements of the THz yield [8] were performed in the range of the pump wavelengths $\lambda_0 = 1.2$–2 μm. The conjoint fit by the function λ_0^{α} of the experimental results [8] and the THz yield at $\lambda_0 = 3.9$ μm measured in [12] provides the dependence of the optics-to-THz conversion efficiency with $\alpha = 2.6$ close to the squared pump wavelength scaling law.The $3D$ + time numerical simulations of the THz emission from the two-color filament with the central wavelength λ_0 varied in the wide range from 0.6 to 10.6 μm [20] showed the optimal efficiency of the conversion into THz radiation at $\lambda_0 = 3$–4 μm. For $\lambda_0 > 4$ μm, the conversion efficiency decreases monotonically. However, the simulations [20] were performed for the fixed ratio between the pulse peak power and the critical power for self-focusing (this results in the increase of the pulse energy from 0.69 mJ at 0.6 μm to 216 mJ at 10.6 μm) and do not account for the optimization of the phase φ [9,21–24] between the harmonics. Thus, it is still debated if the THz energy scaling is proportional to the squared pump wavelength, strictly monotonic, or has the optimal wavelength after which, it tends to decrease. The physical mechanisms that could saturate the λ_0^{α}-scaling law of the THz yield from the two-color filament are still unknown as well.

In this work, we search for the scaling law for the energy of the THz emission from the two-color femtosecond filament formed under the focusing of the pulses with a fixed energy and duration into air. To determine the scaling law, we performed a comprehensive numerical scan over the central wavelengths λ_0 in the range from 0.8 to 8 μm and focusing conditions from the numerical aperture (NA) of 0.006 to 0.03. For each pair of λ_0 and the NA, we identified the maximal THz yield $W_{\mathrm{THz}}^{(\max)}$ corresponding to the optimal phase φ_0 between the fundamental and second harmonics [9,21–23] according to the algorithm proposed in [24,25]. While the harmonics are clearly separated in the spectrum (in our conditions, for NA $\lesssim 0.015$), the dependence of the THz energy $W_{\mathrm{THz}}^{(\max)}$ on the pump wavelength λ_0 is proportional to two competing factors: the free electron energy, which increases with the pump wavelength as λ_0^2, and the total number of free electrons in the filament Q_e, which quasi-exponentially decreases with λ_0. This results in the maximum of the dependence $W_{\mathrm{THz}}^{(\max)}(\lambda_0)$ at the wavelength optimal for the given focusing conditions.

2. Model

We simulated the two-color pulse propagation and THz generation using the unidirectional pulse propagation equation (UPPE) ([26]) for the spatio-temporal harmonic $\widehat{E}(\omega, k_r, z)$ of the axially symmetric electric field $E(t, r, z)$:

$$\left(\frac{\partial}{\partial z} + ik_z\right)\widehat{E}(\omega, k_r, z) = -\frac{2\pi\omega}{c^2 k_z}\widehat{J}(\omega, k_r, z), \tag{1}$$

where t and $\omega = 2\pi\nu$ are the time and angular frequency, z ($k_z = \sqrt{n^2(\omega)\omega^2/c^2 - k_r^2}$) and r (k_r) are the longitudinal and transverse coordinates (projections of the wave-vector), respectively, $n(\omega)$ is the refractive index of dry air, and c is the speed of light.

The material current $J(t, r, z) = \partial P^{(3)}/\partial t + J_{\mathrm{free}} + J_{\mathrm{abs}}$, corresponding to the harmonic $\widehat{J}(\omega, k_r, z)$ accommodates the third-order polarization [27]:

$$P^{(3)}(t) = \chi^{(3)}E^3(t), \tag{2}$$

where $\chi^{(3)}$ corresponds to the Kerr coefficient of air $n_2 = 10^{-19}$ cm^2/W given by ab initio quantum calculations [28], which agrees with the measurements for different pump wavelengths [29,30], the transient photocurrent of free electrons $J_{\mathrm{free}}(t)$ [21] defined as

$$\frac{\partial J_{\text{free}}(t)}{\partial t} = \frac{e^2}{m_e} N_e(t) E(t) - \nu_c J_{\text{free}}(t), \tag{3}$$

where e and m_e are electron charge and mass, $\nu_c \approx 5\ \text{ps}^{-1}$ is the electron-neutral collision rate, and the absorption current responsible for the energy loss due to nonlinear ionization [31]:

$$J_{\text{abs}}(t) = \sum_{\alpha} \frac{W_I^{(\alpha)}}{E(t)} \frac{\partial N_e^{(\alpha)}(t)}{\partial t}, \tag{4}$$

where $W_I^{(\alpha)}$ is the ionization potential of a component, and α is either O_2 or N_2. The free electron density $N_e(t) = \sum_\alpha N_e^{(\alpha)}(t)$ is calculated according to the rate equations:

$$\frac{\partial N_e^{(\alpha)}(t)}{\partial t} = w^{(\alpha)}(E)[\eta_\alpha N_0 - N_e^{(\alpha)}(t)], \tag{5}$$

where $N_0 = 2.7 \times 10^{19}\ \text{cm}^{-3}$ is the neutral density under atmospheric pressure, $\eta_{O_2} = 0.21$, $\eta_{N_2} = 0.79$, $w^{(\alpha)}(E)$ is the tunnel ionization rate:

$$w^{(\alpha)}(E) = 4\omega_a \left(\frac{W_I^{(\alpha)}}{W_H}\right)^{5/2} \frac{E_a}{|E|} \exp\left[-\frac{2}{3}\left(\frac{W_I^{(\alpha)}}{W_H}\right)^{3/2} \frac{E_a}{|E|}\right], \tag{6}$$

where $W_H = 13.6$ eV is the ionization potential of the hydrogen atom, $\omega_a = 41.3\ \text{fs}^{-1}$ is the atomic frequency, and $E_a = 5.17$ GV/cm is the atomic field.

In simulations, we "focus" into air the linearly polarized two-color pulse:

$$E(t, r, z = 0) = e^{-r^2/2a_0^2} \times \left(E_1 e^{-t^2/2\tau_1^2} \cos(\omega_0 t) + E_2 e^{-t^2/2\tau_2^2} \cos(2\omega_0 t + \varphi)\right), \tag{7}$$

where E_1 and E_2 are the amplitudes of the fundamental (ω_0) and second ($2\omega_0$) harmonics; $2\tau_1 = 85$ fs and $2\tau_2 = 125$ fs are the pulse durations of ω_0- and $2\omega_0$-pulses, respectively; φ is the relative phase between them; the input beam diameter is $2a_0 = 3$ mm. To find the wavelength scaling law for the energy of THz radiation W_{THz} emitted from the two-color filament, we considered pulses with several different central wavelengths $\lambda_0 = 2\pi c/\omega_0$ in the range 0.8–8 μm. The energies of ω_0- and $2\omega_0$-pulses were fixed at 1.4 mJ and 10 μJ, respectively, for all pump wavelengths λ_0 studied.

We studied the THz generation for four different focusing conditions: focal lengths of $f = 5$, 10, 15, and 25 cm. The former cases are barely a quasi-collimated propagation, though the vectorial effects such as the longitudinal electric field can still be neglected. For this reason, the *nonparaxial input conditions* [32] in the form [33] were applied to describe the focusing effect. In order to reduce the computational time, we translated the initial conditions from $z = 0$ to $z = z_0 = 4.5$, 9, 12, and 20 cm for $f = 5$, 10, 15, and 25 cm, respectively (see the detailed description of the translation routine in [34]).

The crucial influence of the relative phase φ between ω_0- and $2\omega_0$-pulses on the energy of the THz radiation W_{THz} is well known from both the experiments carried out with $0.8 + 0.4$ μm pulses [9,21–23] and the $0D$ + time photocurrent model [21]:

$$W_{\text{THz}} = A + B \sin(2\varphi - \varphi_0), \tag{8}$$

where A, B, and φ_0 do not vary for the chosen experimental conditions. In the local photocurrent model, $\varphi_0 = 90^\circ$ and $A = B$. UPPE simulations inherit the sine dependence [24], but as soon as they account for the pulse propagation in a nonlinear dispersive medium and integrate the THz yield over the focal volume, φ_0 and the A/B ratio cannot be elucidated prior to the simulations.

Equation (8) includes three unknown constants, A, B, and φ_0. Therefore, to retrieve these parameters, one has to perform three UPPE runs with three different phases $\varphi = \varphi^{(j)}$ (here, $j = 1, 2, 3$) and estimate the THz energy $W_{\mathrm{THz}}^{(j)}$ at the end of the filament for these three phases. For the arbitrary relation between the phases $\varphi^{(j)}$, the values of A, B, and φ_0 can be found from the system of three transcendental equations. In the case of the special choice of the phases between the fundamental and second harmonics $\varphi^{(1)} = 0°$, $\varphi^{(2)} = 60°$ and $\varphi^{(3)} = 120°$, this system has the solution in the elementary functions [24,25]:

$$A = \frac{1}{3}\sum_{j=1}^{3} W_{\mathrm{THz}}^{(j)}, \tag{9}$$

$$B = \sqrt{\frac{2}{3}\sum_{j=1}^{3} (W_{\mathrm{THz}}^{(j)})^2 - 2A^2}, \tag{10}$$

$$\varphi_0 = \mathrm{asin}\left(\frac{A - W_{\mathrm{THz}}^{(1)}}{B}\right). \tag{11}$$

Using the parameters A and B, one can estimate the maximal THz yield for the certain pair (λ_0, f) as $W_{\mathrm{THz}}^{(\max)} = A + B$.

3. Results

The simulated maximal energy $W_{\mathrm{THz}}^{(\max)}$ of the THz radiation is shown in Figure 1 as a function of the pump wavelength λ_0 for all focuses f studied. In the range $\lambda_0 = 0.8$–2 μm, the THz energies are almost the same for any f; however, with the further increase in the wavelength λ_0, the influence of the focusing on the dependence $W_{\mathrm{THz}}^{(\max)}(\lambda_0)$ becomes significant. The THz energy increases monotonically in the range of λ_0 from 0.8 to 8 μm in the case of 5 cm focusing (NA = 0.03). For longer focuses, there is a maximum in the dependence $W_{\mathrm{THz}}^{(\max)}(\lambda_0)$ at ~4 μm for 10 cm (NA = 0.015) focusing and at 1.6–2 μm for 15 cm (NA = 0.01) and 25 cm (NA = 0.006) focusing. In the experiment [8] performed in relatively close conditions (NA ≈ 0.01, $2\tau_1 \approx 72$ fs, pulse energy of 0.4 mJ), the maximum of the THz energy was at $\lambda_0 = 1.8$ μm.

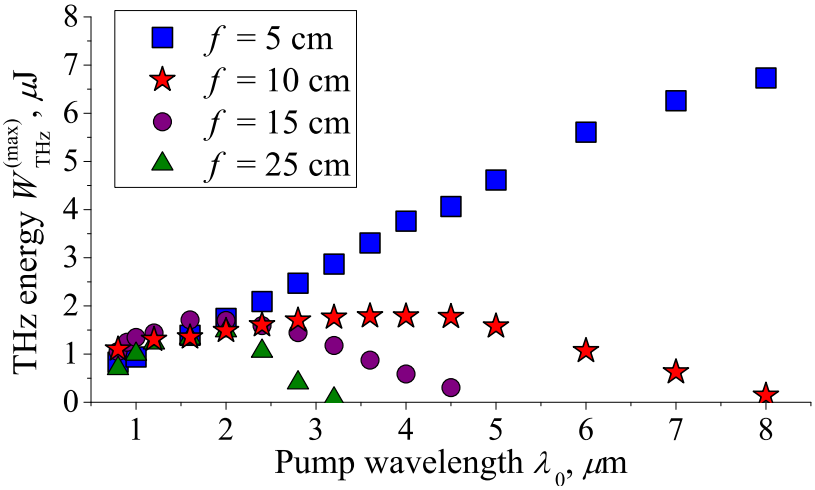

Figure 1. The maximal energy of generated THz radiation $W_{\mathrm{THz}}^{(\max)}$ obtained from UPPE simulations versus the pump wavelength λ_0 for four focal distances: 5 cm (blue squares), 10 cm (red stars), 15 cm (violet circles), and 25 cm (green triangles).

The major mechanism of THz generation from two-color femtosecond filament in gases is the transient photocurrent of free electrons [21,35]. Therefore, the resulting THz energy should depend on the overall amount of free electrons in the plasma channel:

$$Q_e = 2\pi \iint N_e(r,z) r dr dz, \tag{12}$$

where $N_e(r,z)$ is the plasma density remaining after the pulse passes. In our case of the fixed pump pulse energy, for all focusing studied the dependence $Q_e(\lambda_0)$ decreases quasi-exponentially with the increase in the pump wavelength λ_0: $Q_e(\lambda_0) \propto \exp(-\Gamma\lambda_0)$, where Γ depends on the focal distance f (see Figure 2).

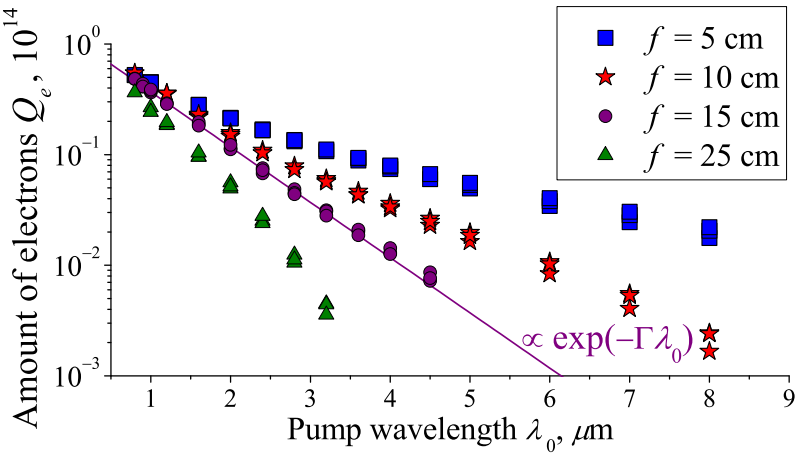

Figure 2. Dependences of the overall amount of free electrons in the filament Q_e (see Equation (12)) on the pump wavelength λ_0 for four focal distances: 5 cm (blue squares), 10 cm (red stars), 15 cm (violet circles), and 25 cm (green triangles). Every pair (λ_0, f) is represented by three points corresponding to three UPPE runs with different phases φ, resulting in a slightly different amount of electrons.

For $f \geq 10$ cm, the dependence $W_{\mathrm{THz}}^{(\max)}(\lambda_0)$ is nonmonotonic (Figure 1). Let us assume $W_{\mathrm{THz}}^{(\max)}(\lambda_0) = Q_e(\lambda_0) \times \mathcal{F}(\lambda_0)$, where $\mathcal{F}(\lambda_0)$ is an unknown function. To provide the maximum in the dependence $W_{\mathrm{THz}}^{(\max)}(\lambda_0)$, the function $\mathcal{F}(\lambda_0)$ should grow up with the increase in the wavelength λ_0 more slowly than the exponential function. Any power function $\mathcal{F}(\lambda_0) \propto \lambda_0^{\alpha}$ with $\alpha > 0$ satisfies this condition; however, only the choice of $\alpha = 2$ is physically justified, since for the fixed pulse intensity, the electron oscillation energy is proportional to λ_0^2.

Figure 3 shows the dependencies of the maximal energy $W_{\mathrm{THz}}^{(\max)}$ of the generated THz radiation on the pump wavelength λ_0 in comparison with $Q_e(\lambda_0)\lambda_0^2$ for four focal distances. For all focuses studied except the shortest one ($f = 5$ cm), these dependencies are in good agreement (cf. the filled and open markers in Figure 3), and the simulated dependencies $W_{\mathrm{THz}}^{(\max)}(\lambda_0)$ can be fit by

$$W_{\mathrm{THz}}^{(\max)} \propto \lambda_0^2 \exp(-\Gamma\lambda_0); \tag{13}$$

see the solid curves in Figure 3a–c.

The proposed fit for the maximal THz energy (13) explains why the λ_0^2-scaling laws cannot be observed in experiments even if the pulse durations, radii, phases, etc., were not changed as the pump wavelength varies. According to Equation (13), the most efficient THz generation is achieved at $\lambda_{\mathrm{opt}} = 2/\Gamma$. Therefore, Equation (13) can be rewritten as $W_{\mathrm{THz}}^{(\max)} \propto \lambda_0^2 \exp\left(-2\lambda_0/\lambda_{\mathrm{opt}}\right)$. The squared pump wavelength factor dominates for $\lambda_0 \ll \lambda_{\mathrm{opt}}/2$. Since the maximum of the dependence $W_{\mathrm{THz}}^{(\max)}(\lambda_0)$ is reached at $\lambda_{\mathrm{opt}} = 2$–$4$ μm, the λ_0^2-scaling of the THz yield could be expected for the pump in the ultraviolet part of spectrum, where the conversion efficiency into the THz range is quite low [36].

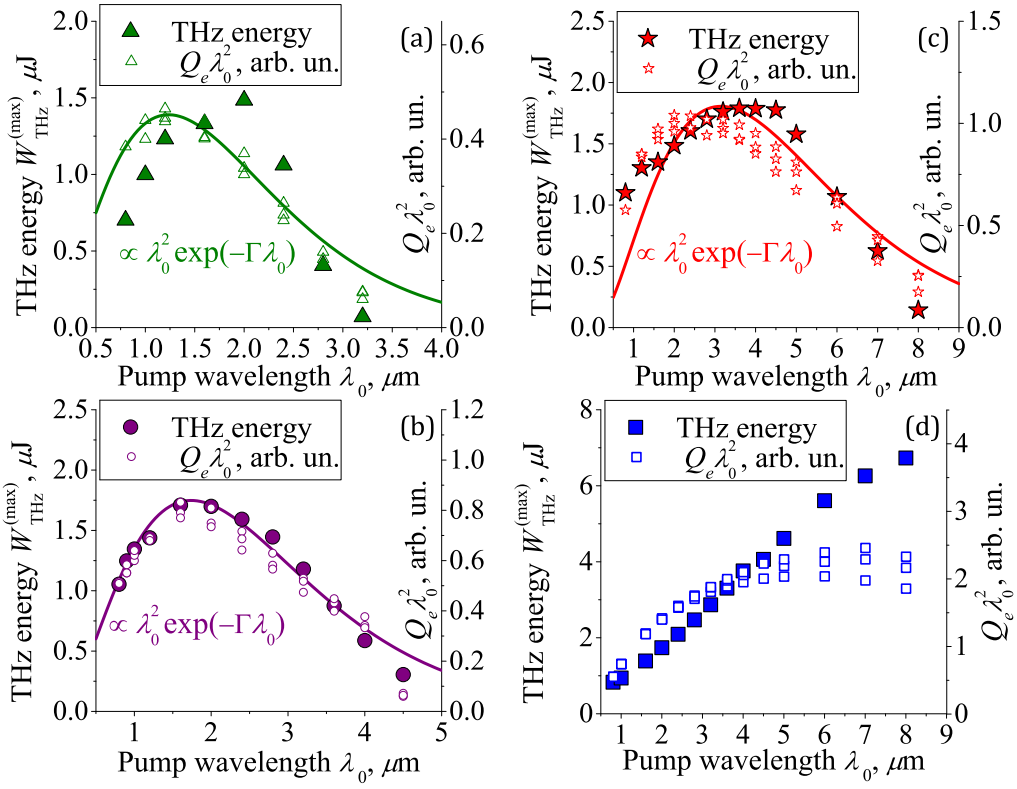

Figure 3. Dependence of the maximal energy of generated THz radiation $W_{\mathrm{THz}}^{(\max)}$ obtained from UPPE simulations on the pump wavelength λ_0 (filled markers) in comparison with $Q_e\lambda_0^2$ (triplets of open markers) for four focal distances: (**a**, green) 25 cm, (**b**, violet) 15 cm, (**c**, red) 10 cm, and (**d**, blue) 5 cm. Solid colored curves show the fits (13).

Let us now return to the case of 5 cm focusing, for which the simulated dependence $W_{\mathrm{THz}}^{(\max)}(\lambda_0)$ qualitatively differs from the rest (see Figure 3): it increases monotonically, despite the dependencies $Q_e(\lambda_0)$ and $Q_e(\lambda_0)\lambda_0^2$ being similar to the other cases; see the blue squares in Figure 2 and the maximum of open squares in Figure 3d at $\lambda_0 \approx 7$ μm. The reason for the discrepancy between the dependencies $W_{\mathrm{THz}}^{(\max)}(\lambda_0)$ and $Q_e(\lambda_0)\lambda_0^2$ could be associated with the features of the pulse field transformation during the propagation. Let us investigate more deeply the pulse spectra at the end of the filament (Figure 4) so as to reveal the reason for such behavior. In the case of $\lambda_0 = 2$ μm for both $f = 5$ and 10 cm, the pulse spectra are similar, except for slightly more broadened harmonics in the spectral domain in the case of 5 cm focusing; see Figure 4a. In contrast, for $\lambda_0 = 8$ μm, the difference between the spectra for the two focusing conditions is significant (Figure 4b). In the case of 5 cm focusing, the optical harmonics are indistinguishable against the supercontinuum background, and the THz generation process is no longer a purely two-color process.

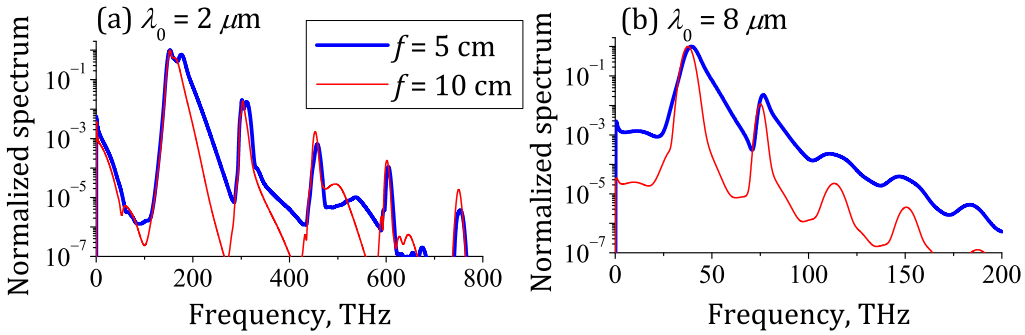

Figure 4. Comparison of the spectra obtained in UPPE simulations at the end of the filament in the case of 5 cm (blue) and 10 cm (red) focusing of the pulses with the central wavelength of (**a**) 2 μm and (**b**) 8 μm.

The explanation of the harmonics vanishing against the supercontinuum is the following. The 0.8 μm filament produces the third harmonic only [37]. In contrast, in the experiment [38] with the 3.9 μm femtosecond filament, the harmonics up to the ninth order (wavelength of ∼0.4 μm) were observed. The pulse with the same wavelength of 3.9 μm generates the third and fifth harmonics during collimated propagation without filamentation [39]. However, while a harmonic is well distinguished, its width in the frequency domain is determined by the initial pulse spectral width and does not decrease while one preserves the ∼100 fs pulse duration. Therefore, the increase in the pulse wavelength results in "denser" localization of the harmonics in the frequency domain. When the pulse intensity reaches the ionization threshold, the harmonics (including the fundamental one) broaden and can overlap with each other, thus forming the multioctave supercontinuum. This effect was observed experimentally for 0.8 μm pump [40] and reproduced in numerical simulations for the 3.9 μm [41] and 10 μm [42] ones. The studies [40–42] were performed in a collimated (or quasi-collimated) geometry of propagation. Therefore, the pulse travels a long distance inside the weakly ionized air. This provides the significant broadening of the spectrum and the vanishing of the harmonics. In our case of 5 cm focusing, the filament's length is ∼6 mm and the comparable spectral broadening of the harmonics occurs due to a much higher ionization degree. For $\lambda_0 = 6$–8 μm, the total number of free electrons for $f = 5$ cm is 5–10-times higher than in the case of $f = 10$ cm (see Figure 2). This difference in the plasma density is enough to overlap the harmonics closely localized in spectrum and make them indistinguishable against the supercontinuum background; see Figure 4.

4. Conclusions

In conclusion, using the self-consistent non-paraxial propagation model with the nonlinear source, which includes the third-order response of bound electrons and the transient photocurrent, we performed a numerical scan over the central wavelengths in the range from 0.8 to 8 μm and focusing conditions from the numerical aperture of 0.006 to 0.03 to determine the scaling law for the energy of THz emission from the two-color femtosecond filament. When the spectral broadening of the optical harmonics is not very large and they are clearly seen above the supercontinuum background, the THz yield is proportional to the total number of free electrons in the filament and the electron oscillation energy. For the fixed two-color pulse parameters, the number of electrons rapidly decreases with the increase in the pulse central wavelength (our simulations showed an exponential decrease). The energy of an electron oscillating in the electromagnetic wave is scaled proportionally to the squared central wavelength. The joint effect of these two competing factors leads to the nonmonotonic scaling law for the THz energy with the maximum at the wavelength 1.6–4 μm, which depends on the focusing conditions.

Author Contributions: I.A.N. performed the numerical simulations; I.A.N., N.A.P., D.E.S., and O.G.K. performed the data analysis and manuscript preparation; A.B.S., W.L., and O.G.K. supervised the whole study. All authors have read and agreed to the published version of the manuscript.

Funding: We thank the financial support from the Russian Science Foundation (grant 20-19-00148). I.A. Nikolaeva acknowledges the scholarship of the Foundation for Advancement in Theoretical Physics and Mathematics "BASIS" (21-2-10-55-1). D.E. Shipilo acknowledges the Scholarship of the Russian Federation President for young scientists (SP-3450.2022.2). Weiwei Liu acknowledges the support from the National Natural Science Foundation of China (Grant 12061131010).

Institutional Review Board Statement: Not applicable.

Informed Consent Statement: Not applicable.

Data Availability Statement: Data underlying the results presented in this paper are not publicly available at this time, but may be obtained from the authors upon reasonable request.

Conflicts of Interest: The authors declare no conflict of interest.

References

1. McKelvy, M.L.; Britt, T.R.; Davis, B.L.; Gillie, J.K.; Lentz, L.A.; Leugers, A.; Nyquist, R.A.; Putzig, C.L. Infrared spectroscopy. *Anal. Chem.* **1996**, *68*, 93–160. [CrossRef]
2. Fuji, T.; Shirai, H.; Nomura, Y. Ultrabroadband mid-infrared spectroscopy with four-wave difference frequency generation. *J. Opt.* **2015**, *17*, 094004. [CrossRef]
3. Woodbury, D.; Feder, L.; Shumakova, V.; Gollner, C.; Schwartz, R.; Miao, B.; Salehi, F.; Korolov, A.; Pugžlys, A.; Baltuška, A.; et al. Laser wakefield acceleration with mid-IR laser pulses. *Opt. Lett.* **2018**, *43*, 1131–1134. [CrossRef]
4. Balcou, P.; Cornaggia, C.; Gomes, A.; Lompre, L.; L'Huillier, A. Optimizing high-order harmonic generation in strong fields. *J. Phys. B* **1992**, *25*, 4467. [CrossRef]
5. Kohler, M.C.; Pfeifer, T.; Hatsagortsyan, K.Z.; Keitel, C.H. Frontiers of atomic high-harmonic generation. In *Advances in Atomic, Molecular, and Optical Physics*; Elsevier: Amsterdam, The Netherlands, 2012; Volume 61, pp. 159–208.
6. Kartashov, D.; Ališauskas, S.; Andriukaitis, G.; Pugžlys, A.; Shneider, M.; Zheltikov, A.; Chin, S.L.; Baltuška, A. Free-space nitrogen gas laser driven by a femtosecond filament. *Phys. Rev. A* **2012**, *86*, 033831. [CrossRef]
7. Panov, N.A.; Shipilo, D.E.; Saletsky, A.M.; Liu, W.; Polynkin, P.G.; Kosareva, O.G. Nonlinear transparency window for ultraintense femtosecond laser pulses in the atmosphere. *Phys. Rev. A* **2019**, *100*, 023832. [CrossRef]
8. Clerici, M.; Peccianti, M.; Schmidt, B.E.; Caspani, L.; Shalaby, M.; Giguere, M.; Lotti, A.; Couairon, A.; Légaré, F.; Ozaki, T.; et al. Wavelength scaling of terahertz generation by gas ionization. *Phys. Rev. Lett.* **2013**, *110*, 253901. [CrossRef]
9. Cook, D.; Hochstrasser, R. Intense terahertz pulses by four-wave rectification in air. *Opt. Lett.* **2000**, *25*, 1210–1212. [CrossRef]
10. Fedorov, V.Y.; Tzortzakis, S. Extreme THz fields from two-color filamentation of midinfrared laser pulses. *Phys. Rev. A* **2018**, *97*, 063842. [CrossRef]
11. Nguyen, A.; de Alaiza Martínez, P.G.; Thiele, I.; Skupin, S.; Bergé, L. Broadband terahertz radiation from two-color mid-and far-infrared laser filaments in air. *Phys. Rev. A* **2018**, *97*, 063839. [CrossRef]
12. Jang, D.; Schwartz, R.M.; Woodbury, D.; Griff-McMahon, J.; Younis, A.H.; Milchberg, H.M.; Kim, K.Y. Efficient terahertz and Brunel harmonic generation from air plasma via mid-infrared coherent control. *Optica* **2019**, *6*, 1338. [CrossRef]
13. Mitrofanov, A.; Sidorov-Biryukov, D.; Nazarov, M.; Voronin, A.; Rozhko, M.; Shutov, A.; Ryabchuk, S.; Serebryannikov, E.; Fedotov, A.; Zheltikov, A. Ultraviolet-to-millimeter-band supercontinua driven by ultrashort mid-infrared laser pulses. *Optica* **2020**, *7*, 15. [CrossRef]
14. Koulouklidis, A.D.; Gollner, C.; Shumakova, V.; Fedorov, V.Y.; Pugžlys, A.; Baltuška, A.; Tzortzakis, S. Observation of extremely efficient terahertz generation from mid-infrared two-color laser filaments. *Nat. Commun.* **2020**, *11*, 1. [CrossRef] [PubMed]
15. Chai, X.; Ropagnol, X.; Ovchinnikov, A.; Chefonov, O.; Ushakov, A.; Garcia-Rosas, C.; Isgandarov, E.; Agranat, M.; Ozaki, T.; Savel'ev, A. Observation of crossover from intraband to interband nonlinear terahertz optics. *Opt. Lett.* **2018**, *43*, 5463–5466. [CrossRef] [PubMed]
16. Nagatsuma, T.; Ducournau, G.; Renaud, C.C. Advances in terahertz communications accelerated by photonics. *Nat. Photon.* **2016**, *10*, 371–379. [CrossRef]
17. Liu, J.; Dai, J.; Chin, S.L.; Zhang, X.C. Broadband terahertz wave remote sensing using coherent manipulation of fluorescence from asymmetrically ionized gases. *Nat. Photon.* **2010**, *4*, 627–631. [CrossRef]
18. Nguyen, A.; Kaltenecker, K.; Delagnes, J.C.; Zhou, B.; Cormier, E.; Fedorov, N.; Bouillaud, R.; Descamps, D.; Thiele, I.; Skupin, S.; et al. Wavelength scaling of terahertz pulse energies delivered by two-color air plasmas. *Opt. Lett.* **2019**, *44*, 1488–1491. [CrossRef]
19. Zhao, H.; Zhang, L.; Huang, S.; Zhang, S.; Zhang, C. Terahertz wave generation from noble gas plasmas induced by a wavelength-tunable femtosecond laser. *IEEE Trans. THz Sci. Tech.* **2018**, *8*, 299–304. [CrossRef]
20. Fedorov, V.Y.; Tzortzakis, S. Optimal wavelength for two-color filamentation-induced terahertz sources. *Opt. Express* **2018**, *26*, 31150. [CrossRef]

21. Kim, K.Y.; Glownia, J.H.; Taylor, A.J.; Rodriguez, G. Terahertz emission from ultrafast ionizing air in symmetry-broken laser fields. *Opt. Express* **2007**, *15*, 4577–4584. [CrossRef]
22. Dai, J.; Karpowicz, N.; Zhang, X.C. Coherent polarization control of terahertz waves generated from two-color laser-induced gas plasma. *Phys. Rev. Lett.* **2009**, *103*, 023001. [CrossRef] [PubMed]
23. Li, M.; Li, W.; Shi, Y.; Lu, P.; Pan, H.; Zeng, H. Verification of the physical mechanism of THz generation by dual-color ultrashort laser pulses. *Appl. Phys. Lett.* **2012**, *101*, 161104. [CrossRef]
24. Solyankin, P.M.; Nikolaeva, I.A.; Angeluts, A.A.; Shipilo, D.E.; Minaev, N.V.; Panov, N.A.; Balakin, A.V.; Zhu, Y.; Kosareva, O.G.; Shkurinov, A.P. THz generation from laser-induced breakdown in pressurized molecular gases: On the way to terahertz remote sensing of the atmospheres of Mars and Venus. *New J. Phys.* **2020**, *22*, 013039. [CrossRef]
25. Nikolaeva, I.; Shipilo, D.; Panov, N.; Kosareva, O. Dual-wavelength filamentation with a fraction of fundamental laser frequency as a wideband THz source. *Laser Phys. Lett.* **2021**, *18*, 025401. [CrossRef]
26. Kolesik, M.; Moloney, J.V. Nonlinear optical pulse propagation simulation: From Maxwell's to unidirectional equations. *Phys. Rev. E* **2004**, *70*, 036604. [CrossRef] [PubMed]
27. Borodin, A.V.; Panov, N.A.; Kosareva, O.G.; Andreeva, V.A.; Esaulkov, M.N.; Makarov, V.A.; Shkurinov, A.P.; Chin, S.L.; Zhang, X.C. Transformation of terahertz spectra emitted from dual-frequency femtosecond pulse interaction in gases. *Opt. Lett.* **2013**, *38*, 1906. [CrossRef]
28. Brown, J.M.; Couairon, A.; Gaarde, M.B. Ab initio calculations of the linear and nonlinear susceptibilities of N_2, O_2, and air in midinfrared laser pulses. *Phys. Rev. A* **2018**, *97*, 063421. [CrossRef]
29. Liu, W.; Chin, S.L. Direct measurement of the critical power of femtosecond Ti:sapphire laser pulse in air. *Opt. Express* **2005**, *13*, 5750. [CrossRef]
30. Zahedpour, S.; Wahlstrand, J.; Milchberg, H. Measurement of the nonlinear refractive index of air constituents at mid-infrared wavelengths. *Opt. Lett.* **2015**, *40*, 5794–5797. [CrossRef]
31. Rae, S.; Burnett, K. Detailed simulations of plasma-induced spectral blueshifting. *Phys. Rev. A* **1992**, *46*, 1084. [CrossRef]
32. Shipilo, D.; Nikolaeva, I.; Fedorov, V.Y.; Tzortzakis, S.; Couairon, A.; Panov, N.; Kosareva, O. Tight focusing of electromagnetic fields by large-aperture mirrors. *Phys. Rev. E* **2019**, *100*, 033316. [CrossRef] [PubMed]
33. Mokrousova, D.; Savinov, S.; Seleznev, L.; Rizaev, G.; Koribut, A.; Mityagin, Y.A.; Ionin, A.; Nikolaeva, I.; Shipilo, D.; Panov, N.; et al. Tracing air-breakdown plasma characteristics from single-color filament terahertz spectra. *J. Infrared Milli Thz Waves* **2020**, *41*, 1105–1113. [CrossRef]
34. Zhang, Z.; Panov, N.; Andreeva, V.; Zhang, Z.; Slepkov, A.; Shipilo, D.; Thomson, M.; Wang, T.J.; Babushkin, I.; Demircan, A.; et al. Optimum chirp for efficient terahertz generation from two-color femtosecond pulses in air. *Appl. Phys. Lett.* **2018**, *113*, 241103. [CrossRef]
35. Andreeva, V.; Kosareva, O.; Panov, N.; Shipilo, D.; Solyankin, P.; Esaulkov, M.; de Alaiza Martínez, P.G.; Shkurinov, A.; Makarov, V.; Bergé, L.; et al. Ultrabroad terahertz spectrum generation from an air-based filament plasma. *Phys. Rev. Lett.* **2016**, *116*, 063902. [CrossRef] [PubMed]
36. Mokrousova, D.; Savinov, S.; Rizaev, G.; Shipilo, D.; Panov, N.; Seleznev, L.; Mityagin, Y.A.; Ionin, A.; Shkurinov, A.; Kosareva, O. Terahertz emission from a single-color ultraviolet filament. *Laser Phys. Lett.* **2019**, *16*, 105403. [CrossRef]
37. Fedotov, A.B.; Koroteev, N.I.; Loy, M.; Xiao, X.; Zheltikov, A.M. Saturation of third-harmonic generation in a plasma of self-induced optical breakdown due to the self-action of 80-fs light pulses. *Opt. Commun.* **1997**, *133*, 587–595. [CrossRef]
38. Mitrofanov, A.V.; Voronin, A.A.; Sidorov-Biryukov, D.A.; Pugžlys, A.; Stepanov, E.A.; Andriukaitis, G.; Ališauskas, S.; Flöry, T.; Fedotov, A.B.; Baltuška, A.; et al. Mid-infrared laser filaments in the atmosphere. *Sci. Rep.* **2015**, *5*, 8368. [CrossRef]
39. Kartashov, D.; Ališauskas, S.; Pugžlys, A.; Voronin, A.A.; Zheltikov, A.M.; Baltuška, A. Third- and fifth-harmonic generation by mid-infrared ultrashort pulses: beyond the fifth-order nonlinearity. *Opt. Lett.* **2012**, *37*, 2268. [CrossRef]
40. Theberge, F.; Liu, W.; Luo, Q.; Chin, S.L. Ultrabroadband continuum generated in air (down to 230 nm) using ultrashort and intense laser pulses. *Appl. Phys. B* **2005**, *80*, 221–225. [CrossRef]
41. Panov, N.A.; Shipilo, D.E.; Andreeva, V.A.; Kosareva, O.G.; Saletsky, A.M.; Xu, H.; Polynkin, P. Supercontinuum of a 3.9-μ m filament in air: Formation of a two-octave plateau and nonlinearly enhanced linear absorption. *Phys. Rev. A* **2016**, *94*, 041801. [CrossRef]
42. Panagiotopoulos, P.; Kolesik, M.; Tochitsky, S.; Koch, S.W.; Moloney, J.V. Two-stage filamentation of 10 μm pulses as a broadband infrared backlighter in the atmosphere. *Opt. Lett.* **2019**, *44*, 3122–3125. [CrossRef] [PubMed]